

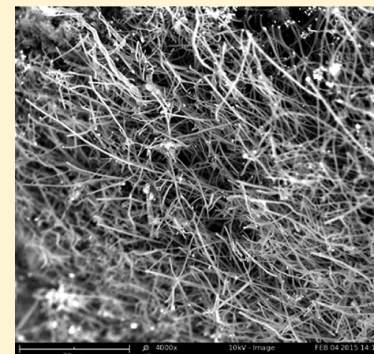
## One-Pot Synthesis of Carbon Nanofibers from CO<sub>2</sub>

Jiawen Ren,<sup>†</sup> Fang-Fang Li,<sup>†</sup> Jason Lau,<sup>†</sup> Luis González-Urbina,<sup>†</sup> and Stuart Licht\*,<sup>†</sup>

<sup>†</sup>Department of Chemistry, The George Washington University, Washington, DC 20052, United States

### S Supporting Information

**ABSTRACT:** Carbon nanofibers, CNFs, due to their superior strength, conductivity, flexibility, and durability have great potential as a material resource but still have limited use due to the cost intensive complexities of their synthesis. Herein, we report the high-yield and scalable electrolytic conversion of atmospheric CO<sub>2</sub> dissolved in molten carbonates into CNFs. It is demonstrated that the conversion of CO<sub>2</sub> → C<sub>CNF</sub> + O<sub>2</sub> can be driven by efficient solar, as well as conventional, energy at inexpensive steel or nickel electrodes. The structure is tuned by controlling the electrolysis conditions, such as the addition of trace transition metals to act as CNF nucleation sites, the addition of zinc as an initiator and the control of current density. A less expensive source of CNFs will facilitate its adoption as a societal resource, and using carbon dioxide as a reactant to generate a value added product such as CNFs provides impetus to consume this greenhouse gas to mitigate climate change.



**KEYWORDS:** Carbon nanofibers, carbon composites, carbon capture, climate change, solar energy

The synthesis of nano carbon fibers and modified CNFs has been of increasing interest, with applications ranging from capacitors, Li-ion batteries, and electrocatalysts to the principal component of lightweight, high strength building materials; today, CNF demand is mainly limited by the complexity and cost of the synthetic process, which requires 30–100-fold higher production energy compared to aluminum.<sup>1,2</sup> Carbon nanofibers have been synthesized from a variety of materials including pitch, rayon, polyacrylonitrile,<sup>3</sup> solid carbon materials,<sup>4,5</sup> acetone,<sup>6</sup> or hydrocarbon gases,<sup>7,8</sup> by employing electrospinning/carbonization, chemical vapor deposition (CVD), arc/plasma techniques,<sup>9,10</sup> etc. Recent interests are focusing on renewable feedstocks, i.e., lignin and cellulose,<sup>11,12</sup> rather than conventional chemicals from the natural gas or petroleum industry. Here, we synthesize a valuable commodity, CNFs, directly from atmospheric CO<sub>2</sub> in a one-pot synthesis. The “production of CNFs by electrolysis in molten lithium carbonate is impossible” according to a prior report in the literature.<sup>13</sup> Yet here, we present exactly that a high yield process for the electrolytic conversion of CO<sub>2</sub>, dissolved in molten carbonates, directly to CNFs at high rates using scalable, inexpensive nickel and steel electrodes. The structure is tuned by controlling the electrolysis conditions, such as the addition of trace nickel to act as CNF nucleation sites, the concentration of added oxide, the addition of zinc as an initiator, and the control of current density. CO<sub>2</sub> is a greenhouse gas that impacts climate change.<sup>14,15</sup> CNFs formed from CO<sub>2</sub>, can contribute to lower greenhouse gases for example by consuming, rather than emitting CO<sub>2</sub>, and by providing a carbon composite material that can be used as an alternative to steel, aluminum, and cement whose productions are associated with massive CO<sub>2</sub> emissions.<sup>16–18</sup> Carbon composites will further decrease emissions by facilitating both

wind turbines and lightweight, low-carbon-footprint transportation.<sup>19</sup>

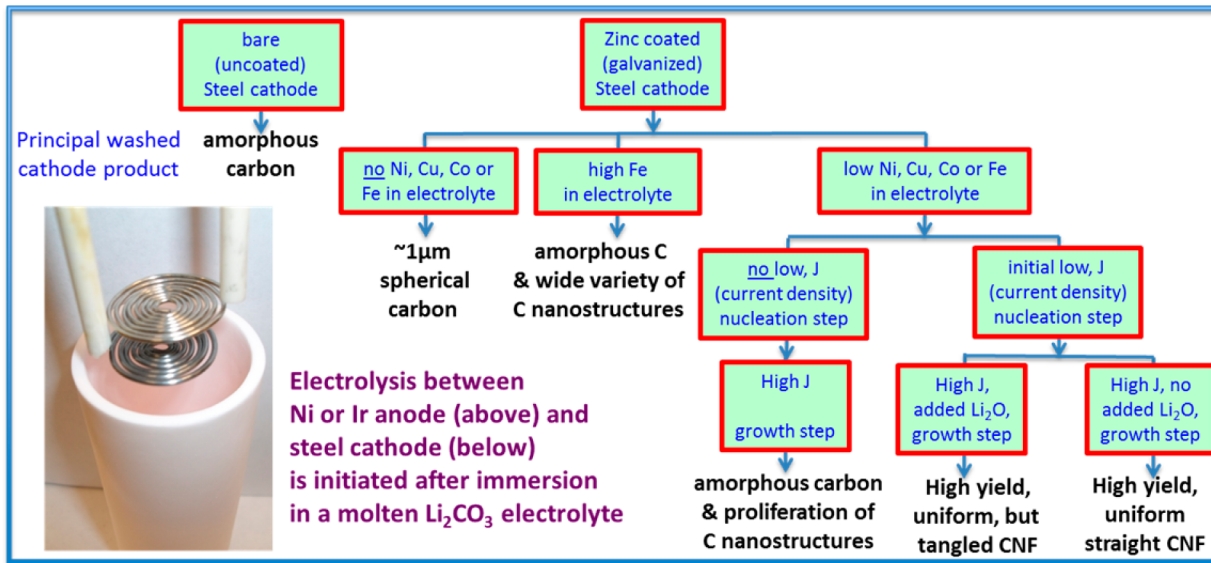
Prior to the recognition of a variety of unique carbon nanoscopic structures such as fullerenes, nanotubes, and nanofibers, the reduction of carbonates to (macroscopic) carbons in inorganic molten electrolytes from hydroxides and a barium chloride/barium carbonate melt was recognized as early as the late 1800s.<sup>20</sup> There are few known routes to the synthesis of carbon nanofibers, and the existing syntheses are energy, equipment, time, and cost-extensive. The electrochemical synthesis of CNFs has not been widely explored. Solid carbon electrodes have been electrolytically converted to nanostructures such as nanotubes in molten halide solutions via alkali metal formation, intercalation into, and exfoliation of the carbon.<sup>5</sup> Instead of the conversion of solid carbon, the rate of the direct reduction of CO<sub>2</sub> studied with carbon and platinum electrodes is limited by the low solubility of CO<sub>2</sub> in molten halides and requires high (15 atm) CO<sub>2</sub> pressure. This conversion is also accompanied by corrosion of the electrodes.<sup>21,22</sup> A study of 5–10% Li<sub>2</sub>CO<sub>3</sub> in molten chloride concluded that “production of CNTs and nanofibers by electrolysis in molten lithium carbonate is impossible” because “reduction and carbon deposition occurred by Li discharge and intercalation into the cathode”.<sup>13</sup> That assessment was correct but did not anticipate the alternative Ni nuclei growth mechanism with zinc initiated paths from molten Li<sub>2</sub>CO<sub>3</sub> observed here.

**Materials and Methods.** Experimental details of the solar thermal electrochemical process, STEP, synthesis of a variety of

**Received:** June 18, 2015

**Revised:** July 16, 2015

**Published:** August 3, 2015

Scheme 1. Molten Carbonate Electrolysis Pathways Converting CO<sub>2</sub> Leading to a High Yield, Uniform CNF Product

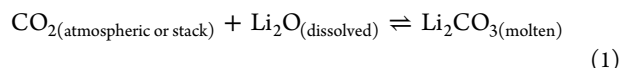
societal staples and carbon capture have been detailed in previous publications.<sup>16–18,23–29</sup> This study focuses primarily on the STEP for carbon electrochemical reactor component to form a high-yield CNF component. Barium carbonate (Alfa Aesar, 99.5%), lithium carbonate (Alfa Aesar, 99%), lithium oxide (Alfa Aesar, 99.5%), and calcium carbonate (Alfa Aesar, 98%) are combined to form various molten electrolytes. Copper(II) and cobalt(II) oxides are from Alfa Aesar, and zinc(II) oxide is from Nanotec.

Electrolyses are driven at a 2.3 A (amp) at the maximum power point of the illuminated concentrator photovoltaic (as shown in Figure S8) or galvanostatically at a set constant current as described in the text. The electrolysis is contained in a pure alumina (AdValue, 99.6%) crucible or pure nickel crucible (Alfa Aesar). Alumina crucible electrolyses used coiled Ni wire (Alfa Aesar, 99.5%) as the (oxygen generating) anode or in scale-up experiments cylinders formed from pure Ni shim (McMaster 9707K5), while electrolyses in the Ni crucibles used the inner walls of the crucible as the anode. Ir anodes were composed of 25 mm × 25 mm × 1 mm 99.7% iridium foil Alfa Aesar 11432 and platinum from Surepure. A wide variety of steel wires for coiled cathodes are effective, an economic form (used in this study) is Fi-Shock 14 gauge, galvanized steel wire model BWC-14200. During electrolysis, the carbon product accumulates at the cathode, which is subsequently removed and cooled. Details of solar (STEP methodology) electrolyses are provided in refs 16, 23, and 25. Subsequent to electrolysis, the product remains on the cathode but falls off when the cathode is extracted, cooled, and uncoiled. The product is washed with either DI water or up to 6 M HCl (both yield similar product, but the latter solution accelerates the washing process) and separated from the washing solution by either paper filtration or centrifugation (both yield similar product, but the latter accelerates the separation process).

The carbon product is washed and analyzed by PHENOM Pro-X energy dispersive spectroscopy on the PHENOM Pro-X SEM; by XRD analysis conducted at a sweep rate of 0.12 degree per minute on a Rigaku Miniflex diffractometer with a 0.01 degree slit width, analyzed using the Jade software package (JADE, 6:1; Materials Data, Inc. Livermore, CA, 2002) and by higher resolution with a Carl Zeiss Sigma VP field emission

scanning electron microscope with energy dispersive X-ray detector. Raman spectroscopy was measured with a LabRAM HR800 Raman microscope (HORIBA) with 532.14 wavelength incident laser light, with a high resolution of 0.6 cm<sup>-1</sup>.

**Results and Discussion.** Here, we show a facile high yield route of carbon nanostructure formation on inexpensive electrodes via molten carbonate electrolysis. The consumed carbonate is directly replaced by absorbed CO<sub>2</sub>. Hence, we show the first demonstration in which this atmospheric carbon dioxide generates carbon nanofibers. Molten carbonates, such as pure Li<sub>2</sub>CO<sub>3</sub> (mp 723 °C) or low melting eutectics such as LiNaKCO<sub>3</sub> (mp 399 °C) or LiBaCaCO<sub>3</sub> (mp 620 °C), mixed with highly soluble oxides, such Li<sub>2</sub>O and BaO, can sustain rapid absorption of CO<sub>2</sub> from atmospheric or stack-exhaust CO<sub>2</sub>. Equilibrium constraining lithium or lithium/barium oxide absorption has been presented, and in the context of atmospheric or smoke stack CO<sub>2</sub> the lithium case is described as<sup>16–18,23</sup>



Scheme 1 presents the successive synthetic variations described in this study that led to the high yield electrolysis of straight uniform CNFs from CO<sub>2</sub> in molten carbonate. Air contains 0.04% CO<sub>2</sub>; this is only  $1.7 \times 10^{-5}$  mol of tetravalent carbon per liter, whereas molten carbonate contains ~20 mol of reducible tetravalent carbon per liter. A separate process to concentrate atmospheric CO<sub>2</sub> is not needed in electrolytic CO<sub>2</sub> to CNF conversion. By absorbing CO<sub>2</sub> from the air, molten carbonates provide a million-fold concentration increase of reducible tetravalent carbon available for splitting (to carbon) in the electrolysis chamber. Carbonate's higher concentration of active, reducible tetravalent carbon sites logarithmically decreases the electrolysis potential and can facilitate charge transfer at low electrolysis potentials. CO<sub>2</sub> is bubbled into the molten carbonate, and during electrolysis, oxygen is evolved at the anode, while a thick solid carbon builds at the cathode (Figure 1).

We observe that carbonate is readily split to carbon approaching 100% Coulombic efficiency (Coulombic efficiency is determined by comparing the moles of applied charge to the

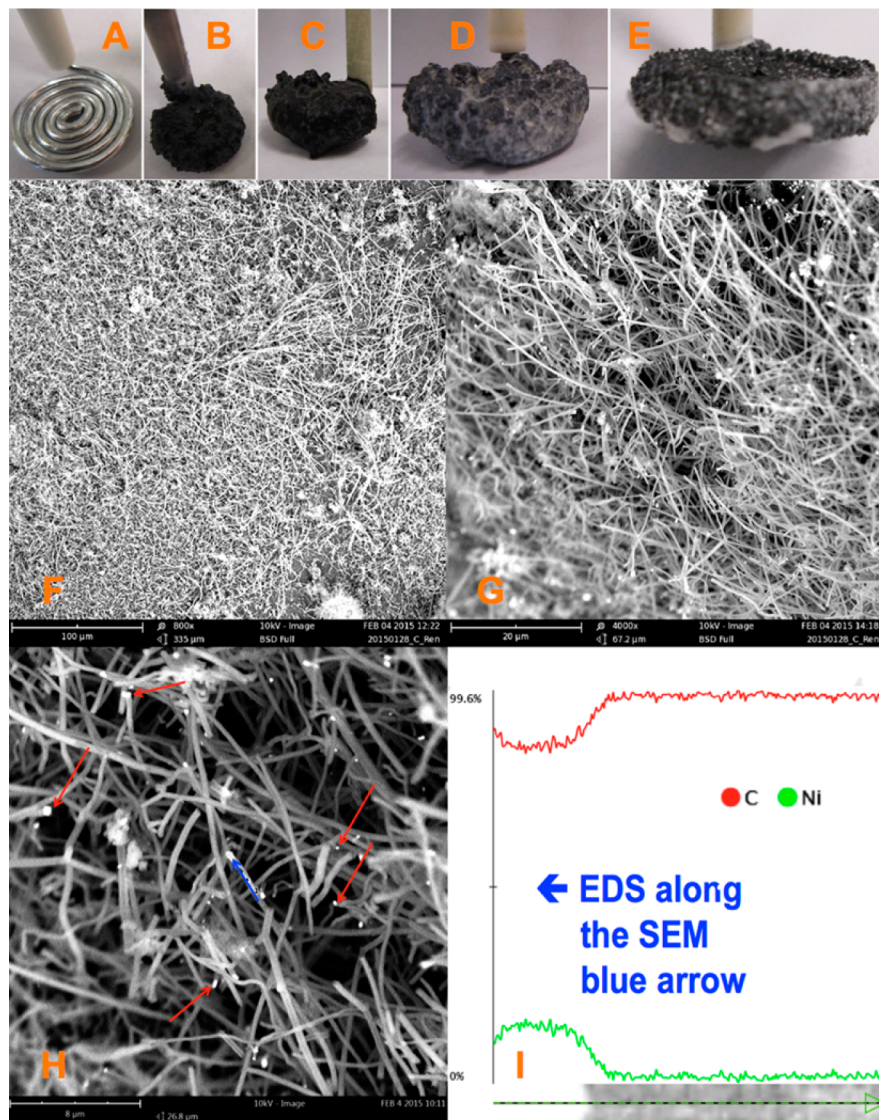
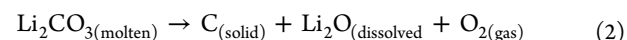


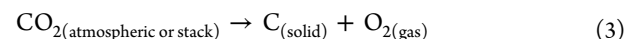
**Figure 1.**  $\text{CO}_2$  to carbon nanofibers formed at a coiled galvanized steel wire cathode with a nickel anode during 0.05 A; then 1 A constant current electrolysis. No  $\text{Li}_2\text{O}$  is added to the 730 °C molten  $\text{Li}_2\text{CO}_3$  electrolyte. SEM F to H are shown at various magnifications of the product removed from the cooled, washed cathode. “A” shows the  $10 \text{ cm}^2$  coiled wire (0.12 cm diameter) cathode prior to electrolysis. The anode is the inner wall of a 20 mL Ni crucible containing the electrolyte. “B–E” exemplify the typical maximum variation of observed cathodes subsequent to removal from carbonate electrolytes after a long (4 Ah) electrolysis in molten carbonate. Red arrows in SEM “H” indicate typical Ni nucleation sites. The blue arrow originates at one Ni site and moves along the CNF path. “I”: EDS composition mapping along the  $6 \mu$  blue arrow path shown in SEM “H”.

moles of product formed, where each mole of solid carbon product formed depends on four moles of electrons;<sup>16–18,23–28</sup> that is unless carbonates are mixed with hydroxides. In the latter case,  $\text{H}_2$  and carbon products are cogenerated.<sup>25</sup> High current densities ( $>1 \text{ A cm}^{-2}$ ) of carbon formation are sustained, and we observe similar sustained currents at carbon, platinum, or steel cathodes (each cathode effectively become a carbon electrode during the product deposition). Full cell electrolysis potentials range from less than 1 V under conditions of higher temperature (e.g., 800 °C), low current density (e.g.,  $\leq 10 \text{ mA cm}^{-2}$ ), and high oxide concentration (e.g., 6 molal  $\text{Li}_2\text{O}$ ), to several volts at high current density (e.g.,  $\geq 500 \text{ mA cm}^{-2}$ ). Conditions that increase carbonate electrolysis voltage are high current density, lower temperature, or lower oxide concentration. Below 800 °C, the product is carbon (and oxygen) and at higher temperatures, the product gradually shifts to a mix of carbon

and (the 2 electron reduction to) carbon monoxide. It becomes pure CO (and  $1/2\text{O}_2$ ) by 950 °C.<sup>24</sup> The  $\leq 800 \text{ }^\circ\text{C}$  four-electron processes is given by



For a net reaction with eq 1:



The cathode product of dissolved carbon dioxide in molten carbonate tends to be an uncontrolled mix of graphites and amorphous carbons (Supporting Information). However, the cathode electrolysis product shown in the SEM of Figure 1 consists of controlled carbon fibers with metal nucleation points (as shown in the figure by EDS using with Ni nucleation). The vast majority of the Ni nanoparticles in the SEM are located at nanofiber tips, while a relative few seem to be aside from, and not associated with, CNF growth. The fibers

are homogeneous throughout the cathode product, characterized by uniform diameters of 200 to 300 nm, and with length of 20 to 200  $\mu\text{m}$ . The fibers are prepared by electrolysis at a 10  $\text{cm}^2$  coiled galvanized steel wire cathode (shown) and an oxygen generating nickel anode in 730 °C molten  $\text{Li}_2\text{CO}_3$ , initiated by a low current of 5  $\text{mA}/\text{cm}^2$  cathode, followed by constant current electrolysis at high current (100  $\text{mA cm}^{-2}$ ) for 2 to 4 Ah. The cooled product consists of fibers mixed with solidified electrolyte. Product readily falls off the cooled cathode when it is uncoiled. The Coulombic efficiency is over 80% (and approaches 100% with carefully recovery of all product after washing); the product (after washing off the electrolyte) consists of >80% pure carbon nanofibers. SEM are shown after washing electrolyte from the product. The washed cathode product is further characterized by X-ray powder diffraction, XRD, and Raman spectroscopy in Figure 2.

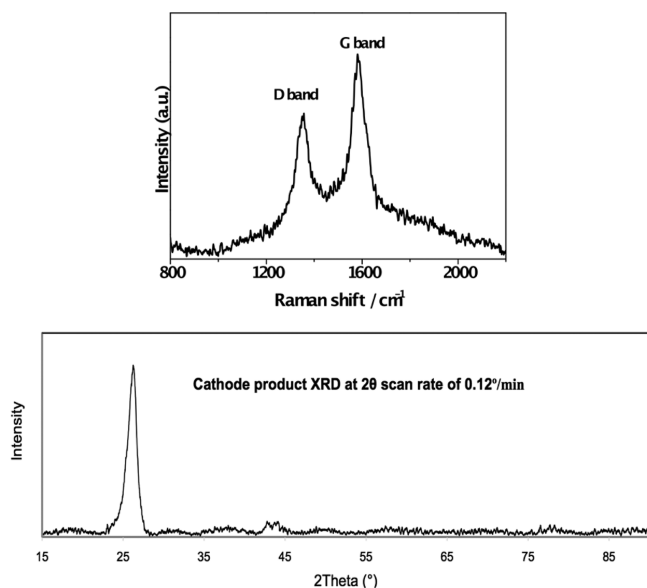


Figure 2. Top: Raman of the carbon products. Bottom: X-ray powder diffraction of the cathode carbon product.

The XRD diffraction peaks in Figure 2 at 26° and 43° are assigned to the hexagonal graphite (002) and diffraction planes (JCPDS card files no. 41-1487) within the CNF (specifically, the stacking of parallel graphene layers and the size of graphene layer, respectively).<sup>19</sup> The resolved XRD peaks at 43° (100 plane) and 44° (101 plane) is evidence of homogeneity of the synthesized CNFs. Raman spectrum was recorded to study the degree of graphitization of the carbon nanofibers. The Raman spectrum exhibits two sharp peaks observed at 1350 and 1580  $\text{cm}^{-1}$ , which correspond to the disorder-induced mode (D band) and the high frequency  $E_{2g}$  first order mode (G band), respectively. The intensity ratio between D band and G band ( $I_D/I_G$ ) is an important parameter to evaluate the graphitization and is 0.70 in our case, which is consistent with commercial hollow carbon nanofiber samples.<sup>30</sup> All of the above information indicates the formation of good CNFs.

In the absence of a nucleating metal, such as Ni, CNFs are not evident during molten electrolysis. This is shown in the Supporting Information in which a Pt or Ir anode is used instead of the Ni electrode. Subsequent to electrolysis in a Ni-free environment ( $\text{Li}_2\text{CO}_3$  at 730 °C with 6 molal  $\text{Li}_2\text{O}$  utilizing either a Pt or Ir, rather than Ni, anode), amorphous and platelet

structures are seen instead of fibers, indicative of partially formed multilayered graphene/graphite structures. Electron dispersive spectroscopy elemental analysis indicates that the amorphous and platelet structures are composed of >99% carbon.

We had not previously anticipated the oxygen-generating anode effects on the structure of the carbon formed at the cathode during carbonate electrolysis. As demonstrated here, these anode effects promote significant carbon nanofiber formation. We have investigated Pt, Ir, and Ni, and each can be effective as molten carbonate oxygen generating anodes.<sup>7,8,23–29</sup> Whereas Ir exhibits no corrosion following hundreds of hours use in molten carbonates, the extent of Ni corrosion is determined by the cation composition of the carbonate electrolyte. A nickel anode undergoes continuous corrosion in a sodium and potassium carbonate electrolyte,<sup>25</sup> it is stable after initial minor corrosion in lithium carbonate electrolytes,<sup>8</sup> and no corrosion of the nickel anode is evident in barium/lithium carbonate electrolytes.<sup>22,25</sup> In lithium carbonate electrolytes, we have quantified the low rate of nickel corrosion at the anode as a function of anode current density, electrolysis time, temperature, and lithium oxide concentration.<sup>17</sup> The Ni loss at a 100  $\text{mA cm}^{-2}$  Ni anode in  $\text{Li}_2\text{CO}_3$  at 750 °C with 0 or 5 molal added  $\text{Li}_2\text{O}$  is respectively 0.5 or 4.1  $\text{mg cm}^{-2}$  of anode subsequent to 600 s of electrolysis and increases to 4.6 or 5.0  $\text{mg cm}^{-2}$  subsequent to 1200 or 5400 s of electrolysis. The Ni loss increases to 7.0 mg or 13.8  $\text{mg cm}^{-2}$ , respectively, subject to higher current (1000  $\text{mA cm}^{-2}$ ) or higher temperature (950 °C). Each of these nickel losses tends to be negligible compared to the mass of Ni used in the various Ni wire or Ni shim configured anodes. Nickel oxide has a low solubility of  $10^{-5}$  mol  $\text{NiO}$  per mol of molten  $\text{Li}_2\text{CO}_3$ ,<sup>31</sup> equivalent to 10 mg Ni per kg  $\text{Li}_2\text{CO}_3$ . This low, limiting solubility constrains some of the corroded nickel to the anode surface as a thin oxide overlayer, with the remainder as soluble oxidized nickel available for reduction and redeposition at the cathode.

The characteristic CNF structure is observed when the electrolysis is initiated at a gradually increasing current density, or with an initial low current (1 h of 5  $\text{mA cm}^{-2}$  at the cathode) followed by an extended high current electrolysis such as at 100  $\text{mA cm}^{-2}$  (for several hours). However, when the electrolysis starts directly at only a high (100  $\text{mA cm}^{-2}$ ) current density. The cathode product is principally amorphous (and only ~25% CNF). The linear EDS map on the middle, right lower side of Figure 1 shows elemental variation along the 6  $\mu\text{m}$  path of the EDS scan from pure Ni at the start of the fiber to pure carbon along the remainder of the fiber. We interpret this mechanistically as follows: due to its low solubility and lower reduction potential, nickel (in this case originating from the anode) is preferentially deposited at low applied electrolysis currents (5 or 10  $\text{mA cm}^{-2}$ ). This is evidenced by the low observed electrolysis voltage (<0.7 V) and sustains the formation of nickel metal cathode deposits, which appear to be necessary to nucleate CNF formation. The high concentration of electrolytic  $[\text{CO}_3^{2-}] \gg [\text{Ni}^{2+}]$  and mass diffusion dictates that higher currents will be dominated by carbonate reduction. The subsequent higher electrolysis voltage thermodynamically required to deposit carbon<sup>24</sup> is only observed at higher applied currents (>20  $\text{mA cm}^{-2}$ ). Hence, without the initial application of low current, amorphous carbon will tend to form, while the CNF structures are readily formed following the low current nickel nucleation activation. The lithium carbonate electrolyte has an abundant Li ion

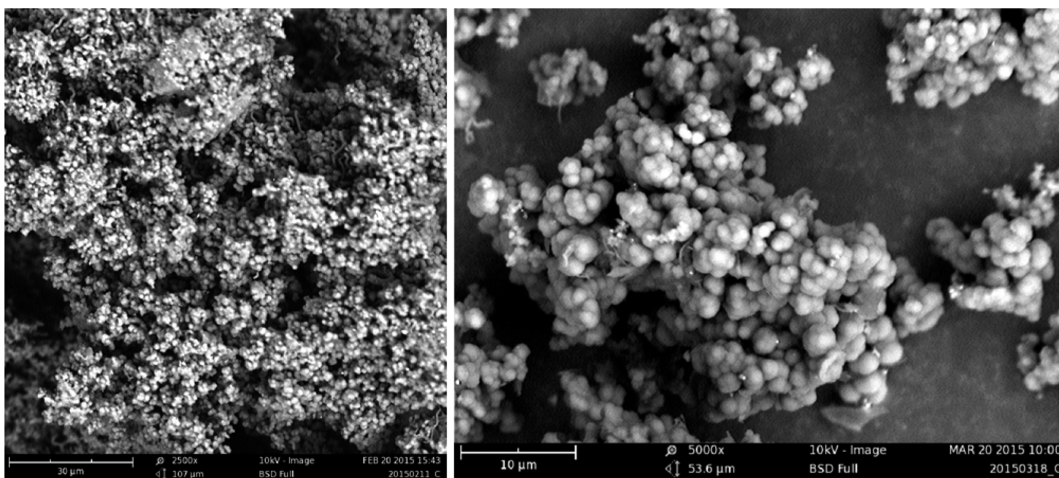


**Figure 3.** Zn effect (without Ni, Co, or Cu) on SEM of the carbon product formed at the cathode following electrolysis in  $\text{Li}_2\text{CO}_3$  (without added  $\text{Li}_2\text{O}$ ) between a planar, square 2.5 by 2.5 cm iridium anode and a coiled wire  $10 \text{ cm}^2$  galvanized (Zn coated) steel cathode. Each electrolysis is conducted at a low initial (0.05A) current to initiate any metal nucleation at the cathode followed by a 1 A electrolysis for 2 h (2 Ah). The observed product is the same without (left side) and with (right side) 0.06 m  $\text{ZnO}$  added to the  $770^\circ\text{C}$  molten  $\text{Li}_2\text{CO}_3$  electrolyte.

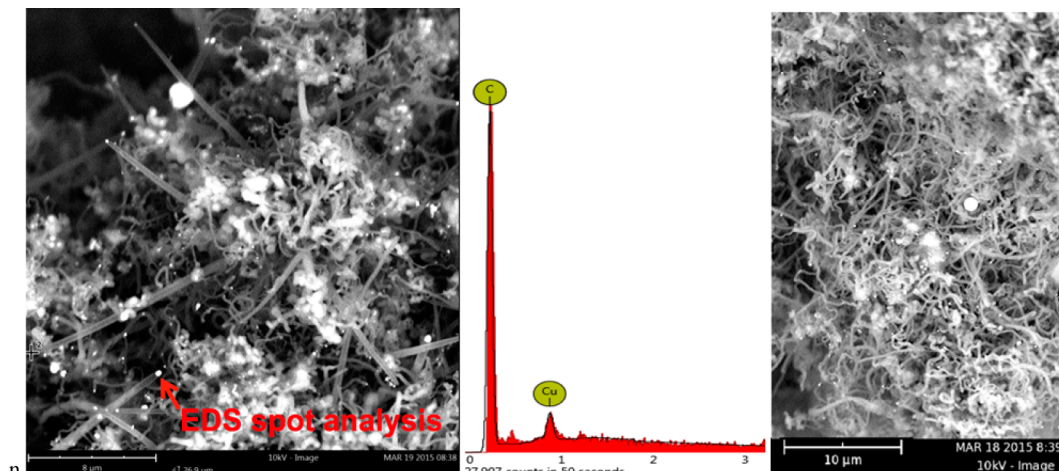


**Figure 4.** Cu or Co effect (without Ni) on SEM of the carbon product formed at the cathode following electrolysis in  $\text{Li}_2\text{CO}_3$  (without added  $\text{Li}_2\text{O}$ ) between a planar, square 2.5 by 2.5 cm iridium anode and a coiled wire  $10 \text{ cm}^2$  galvanized (Zn coated) steel cathode. Top: with 0.06 m  $\text{CuO}$ ; bottom right: with 0.06 m  $\text{CoO}$  added to the  $770^\circ\text{C}$  molten  $\text{Li}_2\text{CO}_3$  electrolyte. Bottom: left EDS analysis of spot shown from the  $\text{CuO}$  cathode product. Each electrolysis is conducted at a low initial (0.05) current to initiate any metal nucleation at the cathode followed by a 1 A electrolysis for 2 h (2 Ah).

concentration, and we see no evidence that Li ion intercalation interferes with the CNF growth. Li intercalation can still occur, but not the explosive exfoliation of the graphite associated with lithium metal deposition (the applied potential is too low to allow Li metal growth).

Rather than the *straight, uniform diameter* CNFs observed in Figure 1, when  $\text{Li}_2\text{O}$  is added to the molten  $\text{Li}_2\text{CO}_3$  electrolyte the electrolysis product is a proliferation of *tangled* CNFs of a *wide variety of diameters* as shown in the *Supporting Information*. Evidently, high concentrations of oxide localized in the CNF formation region leads to torsional effects (tangling).

The cathode consists of galvanized (zinc coated) steel. This zinc metal is a critical activator to the observed high-yield CNF production but acts in a manner different than the nickel metal type of nucleation. Unlike Ni, Zn melts at  $420^\circ\text{C}$  and is a liquid at the electrolysis temperature. Figure 3 presents the action of Zn (in the absence of nickel), whether present only as zinc metal on the galvanized steel cathode surface, or additionally as

added as 0.06 m  $\text{ZnO}$  to the molten  $\text{Li}_2\text{CO}_3$  electrolyte on the carbon nanostructures formed at the cathode. In either case, carbon is formed on a  $10 \text{ cm}^2$  cathode as photographed in the top left of Figure 1, but the anode instead of nickel is a planar  $6.3 \text{ cm}^2$  square iridium electrode. The observed cathode product conformation consists of spherical  $\sim 1 \mu\text{m}$  carbon structures gathered in 3 to  $6 \mu\text{m}$  clusters. In addition, a small fraction (<10%) of the washed product is seen to contain CNFs. *In the absence of zinc* (using either iron or nongalvanized steel cathodes) but in the presence of nickel, produced amorphous graphites and uncontrolled nanofiber structures with diameters ranging from 0.2 to  $4 \mu\text{m}$  and either circular or rectangular duct-like cross sections as shown in the *Supporting Information*.

Figure 4 presents evidence that in addition to Ni, Cu and Co can also act as nucleation sites in the high yield formation of CNFs at the cathode during electrolysis of molten carbonates. Each electrolyte yields CNFs. In the top SEM of the  $\text{CuO}$  cathode product, EDS analysis of the bright spot shown at the

beginning of the carbon nanofiber exhibits pure copper and carbon, providing evidence that the deposited copper acts as a nucleation point to initiate CNF formation. Each of the nucleation metals which we have observed that promote CNF growth have in common that they require a low reduction/deposition potential (which is less than that required for carbon growth) and lead to higher CNF yield when deposited from low concentrations at low electrochemical current density. This range of metals including nickel, copper, iron, and cobalt enhancing the high yield production of CNFs by molten electrolysis correlates with the metals that catalyze CVD growth of CNFs.<sup>10,19</sup>

As observed in Figures 1 and 4, and as further delineated in the Supporting Information, Ni, Cu, Co, or Fe nucleates the high-yield, high-rate production of carbon nanofiber formation in the presence of zinc metal. However, little or uncontrolled CNF formation is observed in the absence of zinc. In each of the prior experiments, zinc metal (which melts at 420 °C) is present in the form of the coating over the steel cathode formed from conventional, galvanized steel wire. A high fraction of the carbon product is consistently CNFs when galvanized (with zinc) steel is used as the cathode and is not when either iron wire or 316 stainless steel shim was employed as the cathode.

As noted, we observe that electrolyses initiated at a high current generated a profusion of amorphous graphites, and a variety of carbon nanostructures rather than a high yield of nanofibers, while electrolyses initiated with a low current step prior to the high current can generate a high yield of uniform CNFs. Deposition of Ni, Co, Cu (or Fe) at low current density, from electrolytes which have a low concentration of the metal, dissolved as the oxide, lead to small, isolated nucleation sites on the cathode, as evidenced by EDS, which promote CNF growth. A solid metal cathode does not have these characteristics and does not lead to homogeneous CNF growth. As seen in the SI, an overabundance of Fe leads to uncontrolled growth, which in the extreme would tend toward an undefined randomly distributed (amorphous) carbon. Combined with an absence of zinc metal, the absence of this low current step produced amorphous graphites (Supporting Information) or a profusion of nanofiber structures (Supporting Information) with diameters ranging from 0.2 to 4 μm and either circular or rectangular duct-like cross sections. It will be of interest in future studies to isolate conditions that refine the distribution of these different structures. As previously noted, the low current step occurs at a potential of <0.7 V, which is sufficient to form metal nucleation sites at the cathode, but is thermodynamically energetically insufficient to reduce carbonate to solid carbon.

A proposed mechanism of the observed high yield CNF that is consistent with the observed zinc activation and metal nucleation effects is presented and the observation that the STEP CNF electrolysis chamber is readily scalable are described in the Supporting Information. The demonstrated CNF synthesis can be driven by any electric source. As an alternative to conventionally generated electrical, we have also driven the CNF synthesis using electric current as generated by an illuminated efficient concentrator photovoltaic operating at maximum power point (SI).

**Conclusions.** Here, we show a new high yield pathway to produce carbon nanofibers directly from atmospheric or exhaust CO<sub>2</sub> in an inexpensive molten electrolysis. Formation of a highly valued, compact, readily stored form of carbon

directly from carbon dioxide may provide a new pathway to mitigate this greenhouse gas. Today, carbon nanofibers require 30- to 100-fold higher production energy compared to aluminum production. We present the first high yield, inexpensive synthesis of carbon nanofibers from the direct electrolytic conversion of CO<sub>2</sub>, dissolved in molten carbonates to CNFs at high rates using scalable, inexpensive nickel and steel electrodes. The structure is tuned by controlling the electrolysis conditions, such as the addition of trace nickel to act as CNT nucleation sites, limits to the electrolytic oxide concentration, inclusion of zinc, and control of current density. New infrastructure and merchandise built from CNFs would provide a repository to store atmospheric CO<sub>2</sub>. The Raman, XED, and SEM characterization provides fundamental evidence of the high yield and purity of the CNF synthesis. Future papers will explore application level testing of the strength, thermal, and electrical conductivities and lithium ion intercalation properties of the CNFs synthesized from CO<sub>2</sub> in molten salts tuned for applications under various electrochemical conditions. It is evident in the Supporting Information that a range of carbon nanostructures is attainable and future studies will probe conditions to characterize and optimize growth of these structures.

## ■ ASSOCIATED CONTENT

### ● Supporting Information

The Supporting Information is available free of charge on the ACS Publications website at DOI: [10.1021/acs.nanolett.5b02427](https://doi.org/10.1021/acs.nanolett.5b02427).

- (i) Conventional CO<sub>2</sub> to carbon formation in carbonates,
- (ii) Ni catalyzed CO<sub>2</sub> to CNF formation, (iii) other metals' action on molten electrolytic carbon formation,
- (iv) a mechanism of high yield electrolytic CNF formation, (v) scalability of the CNT formation, and
- (vi) high rate CO<sub>2</sub> splitting in carbonates at high solar efficiency ([PDF](#))

## ■ AUTHOR INFORMATION

### Corresponding Author

\*E-mail: [slicht@gwu.edu](mailto:slicht@gwu.edu).

### Notes

The authors declare no competing financial interest.

## ■ ACKNOWLEDGMENTS

This project was supported in part by a grant from the United States National Science Foundation 1230732. We are grateful to the Director of the George Washington University Institute for Nanotechnology Prof. Michael Keidar and his research group members Dr. Alexey Shashurin and Xiuqi Fang for their help in attaining the Raman spectroscopy.

## ■ REFERENCES

- (1) pluscomposites, *Composites: Materials of the Future: Part 4: Carbon fibre reinforced composites*, at: <http://www.pluscomposites.eu/publications>, directly accessed July 16, 2015 at: [http://www.pluscomposites.eu/sites/default/files/Technical%20series%20-%20Part%204%20-%20Carbon%20fibre%20reinforced%20composites\\_0.pdf](http://www.pluscomposites.eu/sites/default/files/Technical%20series%20-%20Part%204%20-%20Carbon%20fibre%20reinforced%20composites_0.pdf).
- (2) Kim, H. C.; Fthenakis, V. J. *Ind. Ecol.* **2013**, *17*, 528–541.
- (3) Greiner, A.; Wendorff, J. H. *Angew. Chem., Int. Ed.* **2007**, *46*, 5670–5703.
- (4) Shen, Y.; Yan, L.; Song, H.; Yang, J.; Yang, G.; Chen, X.; Zhou, J.; Yu, Z.-Z.; Yang, S. *Angew. Chem., Int. Ed.* **2012**, *51*, 12202–12205.

- (5) Hsu, W. K.; Hare, J. P.; Terrones, H. W.; Kroto; Walton, D. R. M. *Nature* **1995**, *377*, 687.
- (6) Kodumagulla, A.; Varanasi, V.; Perace, R. C.; Wu, W. C.; Hensley, D. K.; Tracey, J. B.; McKnight, T. E.; Melechko, A. V. *Nanomater. Nanotechnol.* **2014**, *115*, 1464–1473.
- (7) Vander Wal, R. L.; Hall, L. J. *Chem. Phys. Lett.* **2001**, *349*, 178–184.
- (8) Mahammadunnisa, S.; Reddy, E. L.; Ray, D.; Subrahmanyam, C.; Whitehead, J. C. *Int. J. Greenhouse Gas Control* **2013**, *16*, 361–363.
- (9) Iijima, S. *Nature* **1991**, *354*, 56–58.
- (10) Ebbesen, T. W.; Ajayan, P. M. *Nature* **1992**, *358*, 220–222.
- (11) Lallave, M.; Bedia, J.; Ruiz-Rosas, R.; Rodríguez-Mirasol, J.; Cordero, T.; Otero, J. C.; Marquez, M.; Barrero, A.; Loscertales, I. G. *Adv. Mater.* **2007**, *19*, 4292–4296.
- (12) Wu, A.-Y.; Li, C.; Liang, H.-W.; Chen, J.-F.; Yu, S.-H. *Angew. Chem., Int. Ed.* **2013**, *52*, 2925–2929.
- (13) Dimitrov, A. T. *Maced. J. Chem. Chem. Eng.* **2009**, *28*, 111–118.
- (14) Bardgett, R. D.; Putten, W. H. *Nature* **2014**, *515*, 505–511.
- (15) Giosan, L.; Syvitski, J.; Constantinescu, J.; Day, J. *Nature* **2014**, *516*, 31–33.
- (16) Licht, S. *Adv. Mater.* **2011**, *23*, 5592–5612.
- (17) Licht, S.; Wu, H. *J. Phys. Chem. C* **2011**, *115*, 25138–25157.
- (18) Licht, S.; Wu, H.; Hettige, C.; Wang, B.; Lau, J.; Asercion, J.; Stuart, J. *Chem. Commun.* **2012**, *48*, 6019–6021.
- (19) Song, Y.; Youn, J.; Gutowski, T. *Composites, Part A* **2009**, *40*, 1257–1265.
- (20) Burkhardt, Z. *Z. Chem.* **1870**, *13*, 213. as referenced in Haber, F.; Tolloczko, St. Z. *Anorg. Chem.* **1904**, *41*, 407.
- (21) Dimitrov, A.; Tomova, A.; Grozdanov, A.; Popovski, O.; Paunović, P. *J. Solid State Electrochem.* **2013**, *17*, 399–407.
- (22) Novoselova, I.; Oliinyk, N.; Voronina, F.; Volkov, S.; Konchits, A.; Yanchuk, I.; Yefanov, V.; Kolesnik, S.; Darpet, M. *Phys. E* **2008**, *40*, 2231–2237.
- (23) Licht, S.; Cui, B.; Wang, B. *J. CO<sub>2</sub> Utilization* **2013**, *2*, 58–63.
- (24) Licht, S.; Wang, B.; Ghosh, S.; Ayub, H.; Jiang, D.; Ganley, J. *J. Phys. Chem. Lett.* **2010**, *1*, 2363–2368.
- (25) Li, F.-F.; Liu, S.; Cui, B.; Lau, J.; Stuart, J.; Wang, B.; Licht, S. *Adv. Energy Materials* **2015**, *5*, 1–7.
- (26) Licht, S. *J. Phys. Chem. C* **2009**, *113*, 16283–16292.
- (27) Cui, B.; Licht, S. *Green Chem.* **2013**, *15*, 881–884.
- (28) Licht, S.; Wang, B. *Chem. Commun.* **2010**, *46*, 7004–7006; **2011**, *47*, 3081–3083.
- (29) Licht, S.; Cui, B.; Wang, B.; Li, F.-F.; Lau, J.; Liu, S. *Science* **2014**, *345*, 637–640.
- (30) Saravanan, M.; Sennu, P.; Ganesan, M.; Ambalavan, S. *J. Electrochem. Soc.* **2012**, *160*, A70–A76.
- (31) Ota, K.; Mitsuima, S.; Kato, S.; Asano, S.; Yoshitake, H.; Kaymiya, N. *J. Electrochem. Soc.* **1992**, *139*, 667–671.